Bioturbating animals control the mobility of redox-sensitive trace elements in organic-rich mudstone

Dario Harazim[1]*, Duncan McIlroy[1], Nicholas P. Edwards[2,3], Roy A. Wogelius[2,3], Phillip L. Manning[2,4], Kristin M. Poduska[5], Graham D. Layne[1], Dimosthenis Sokaras[6], Roberto Alonso-Mori[6], and Uwe Bergmann[6]

[1]Department of Earth Sciences, Memorial University of Newfoundland, St. John's, Newfoundland A1B 3X5, Canada
[2]School of Earth, Atmospheric, and Environmental Sciences, University of Manchester, Manchester M13 9PL, UK
[3]Williamson Research Centre for Molecular and Environmental Science, University of Manchester, Manchester M13 9PL, UK
[4]Department of Geology and Environmental Geosciences, College of Charleston, 66 George Street, Charleston, South Carolina 29424, USA
[5]Department of Physics and Physical Oceanography, Memorial University of Newfoundland, St. John's, Newfoundland A1B 3X7, Canada
[6]SLAC National Accelerator Laboratory, Menlo Park, California 94025, USA

ABSTRACT

Bioturbating animals modify the original mineralogy, porosity, organic content, and fabric of mud, thus affecting the burial diagenetic pathways of potential hydrocarbon source, seal, and reservoir rocks. High-sensitivity, synchrotron rapid scanning X-ray fluorescence elemental mapping reveals that producers of phycosiphoniform burrows systematically partition redox-sensitive trace elements (i.e., Fe, V, Cr, Mn, Co, Ni, Cu, and As) in fine-grained siliciclastic rocks. Systematic differences in organic carbon content (total organic carbon >1.5 wt%) and quality ($\Delta^{13}C_{org}$ ~0.6‰) are measured between the burrow core and host sediment. The relative enrichment of redox-sensitive elements in the burrow core does not correlate with significant neo-formation of early diagenetic pyrite (via trace metal pyritization), but is best explained by physical concentration of clay- and silt-sized components. A measured loss (~–15%) of the large-ionic-radius elements Sr and Ba from both burrow halo and core is most likely associated with the release of Sr and Ba to pore waters during biological (*in vivo*) weathering of silt- to clay-sized lithic components and feldspar. This newly documented effect has significant potential to inform the interpretation of geochemical proxy and rock property data, particularly from shales, where elemental analyses are commonly employed to predict reservoir quality and support paleoenvironmental analysis.

INTRODUCTION

Bulk-rock geochemical interpretation of organic-rich mudstones is fundamental to geological models of both hydrocarbon systems (Ratcliffe et al., 2012) and oceanic anoxic events (Jenkyns, 2010). This study documents for the first time the effects of deposit-feeding organisms on the spatial (centimeter to decimeter scale) patterns and characteristics of redox-sensitive trace elements in bioturbated siliciclastic mudstone. Bioturbation has hitherto been modeled as a predominantly physical phenomenon that facilitates oxidation of buried organic matter and metal sulfides, thereby driving trace elements into solution (Aller and Rude, 1988). The incomplete understanding of the effects of bioturbation on sediment biogeochemistry is a significant shortcoming of such models, especially because most whole-rock geochemical and compositional data sets use destructive sampling that mixes sedimentary components of dissimilar origin (e.g., Hesselbo et al., 2007). Quantifying the spatial chemical heterogeneity of fine-grained sedimentary rocks on a centimeter scale (Zhu et al., 2006) is critical if we are to place constraints on mass transfer between sediment fabrics and thereby contribute to the understanding about the origin of directional shale anisotropy at a range of scales (cf. Hart et al., 2013). Conventional scanning electron microscope (SEM)–based energy dispersive X-ray spectroscopy techniques for surface compositional mapping are very slow (~12 h/cm^2), limiting the area that can be analyzed during one continuous sample run (cf. Edwards et al., 2014). Nondestructive synchrotron rapid scanning X-ray fluorescence (SRS-XRF) elemental mapping images the spatial distribution of both mineralized and amorphous inorganic products of organic matter remineralization (i.e., carbonates, silicates, phosphates, and metal sulfides) at a range of scales (Wogelius et al., 2011). SRS-XRF maps are integrated with conventional organic and inorganic geochemistry to elucidate the effect of grain-selective deposit feeding on elemental distribution, sediment mineralogy, and both the composition and abundance of organic matter.

METHODS

Geological Background and Sampling Strategy

Phycosiphoniform burrows (Fig. 1) are the earliest component of the studied ichnofabric from the Cretaceous turbidites of the Rosario Formation (Baja California, Mexico) (Callow et al., 2013, their figure 5A). Large (5 kg) samples with phycosiphoniform trace fossils were collected from fresh sandstone and mudstone outcrops in channel overbank deposits (Callow et al., 2013; Fig. 2B) and slabbed to remove any effects of surface weathering. The large phycosiphoniform burrows enabled sufficient

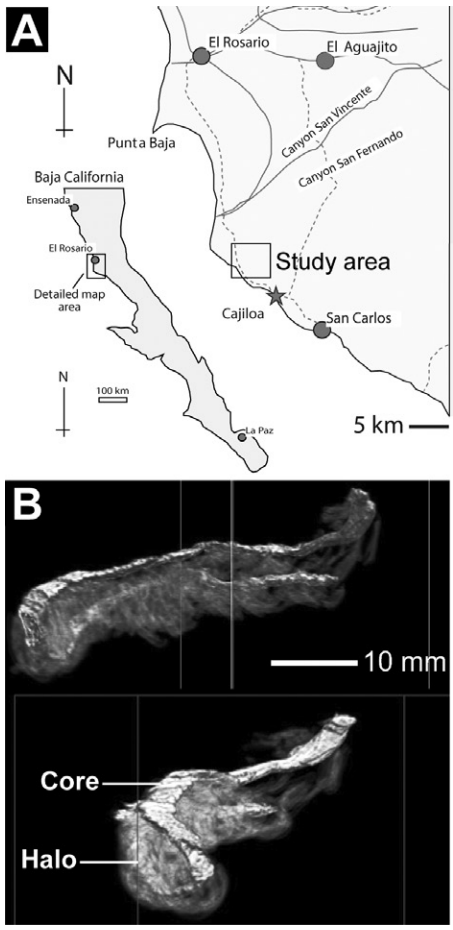

Figure 1. A: Location map of sampling area near Rosario (Baja California, Mexico). B: Three-dimensional reconstruction of burrow halo and core by an unknown vermiform organism (after Bednarz and McIlroy, 2009).

*Current address: Chevron Energy Technology Company, 1500 Louisiana Street, Houston, Texas 77002, USA; E-mail: harazimdario@gmail.com.

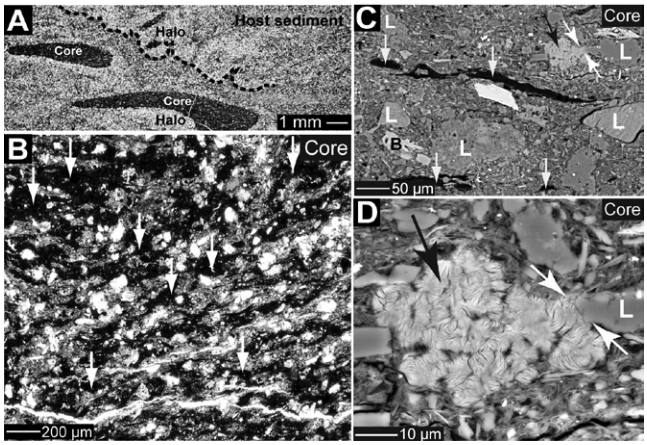

Figure 2. A: Low-power thin-section micrograph (plane-polarized light) showing phycosiphoniform burrow elements halo and core (perpendicular to bedding). Light, sand-rich halo is usually located beneath dark, clay-rich fecal core. Diameter of burrow core is ~5 mm. B: Thin-section micrograph (plane-polarized light) of the burrow core. Note the comparatively high concentration (total organic carbon [TOC] 1.8 wt%; Fig. 3) of organic matter (white arrows) within the clay-rich burrow core. C: Backscattered scanning electron microscope image of the burrow core. Burrow core contains some silt-sized lithic components >40 µm (indicated as "L") and minor biotite ("B") within predominantly illitic and/or chloritic matrix. Larger (>50 µm in length) elongated, curvilinear assemblages of organic carbon (vertical white arrows) are very common within the burrow core. D: High-resolution micrograph of the burrow core in B shows partial replacement of weathering-susceptible lithic clasts or feldspar (black arrow) by fibrous illite and/or smectite (white arrows mark replacement front).

material for analysis to be collected from the different burrow components using a handheld rotary drill. The sample powder was analyzed via X-ray diffraction (XRD) and Fourier transform infrared analysis (FTIR) (see Poduska et al., 2011) to determine composition and to exclude chemical diagenesis as a potential source of uncertainty. Host sediment, halo, and core were analyzed for weight percentage (wt%) of total organic carbon (TOC) using a Carlo Erba elemental analyzer. All compositional analyses (except solution inductively coupled plasma–mass spectrometry [ICP-MS] analyses) were carried out on the same aliquot. Additional powder samples were obtained from fresh surfaces using a stationary high-precision micro mill. These powders were geochemically analyzed via ICP-MS (see Jenner et al., 1990).

Chemical Imaging via SRS-XRF

Non-destructive SRS-XRF imaging (Fig. 3) was performed at wiggler beam line 6-2 at the Stanford Synchrotron Radiation Lightsource (Menlo Park, California, USA). Spatial elemental maps were acquired with incident X-ray beam energies of 12 and 3.15 keV to image elements of high (Ca to As K-emission) and low (Al to K K-emission) atomic weight, respectively, using a 100 µm tantalum pinhole that generated a similar beam spot size. Flux was calculated to be between 10^{10} and 10^{11} photons s^{-1} at high *Z* (high atomic weight elements), and ~10^{9} photons s^{-1} at low *Z*. High-*Z* experiments were carried out under ambient conditions. Low-*Z* experiments were carried out with specimens enclosed within a helium atmosphere in order to avoid X-ray absorption and the scattering effects of air at low incident beam energy (see Edwards et al., 2014).

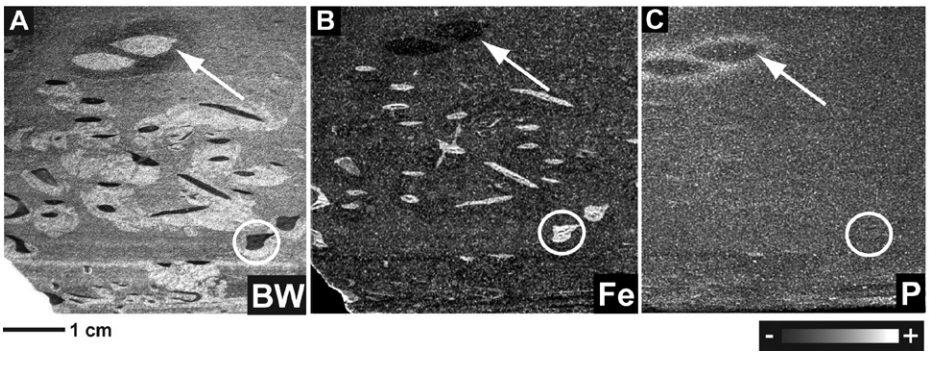

Figure 3. Synchrotron rapid scanning X-ray fluorescence (SRS-XRF) elemental maps resolving details of elemental distribution and relative concentrations with respect to biogenic structures. A: Optical (black and white, BW) photograph of prominent sample containing large (>5 mm) phycosiphoniform traces (circle) as well as *Planolites* isp. (arrow). B: SRS-XRF map of iron. Data collected at beam line 6-2 at Stanford Synchrotron Radiation Lightsource (SSRL; Menlo Park, California, USA); beam energy/size/flux/detector distance = 12 keV/100 µm/10^{11} photons s^{-1}/~120 mm. C: SRS-XRF map of phosphorus. Data collected at beam line 6-2 at SSRL; beam energy/size/flux/detector distance = 3keV/100 µm /10^{9} photons s^{-1}/~10 mm. Active detector area ~50 mm^2.

RESULTS

Visual estimates of porosity using transmitted light microscopy reveal a post-compaction porosity of up to 30% in the burrow halo (Fig. 2A). Grain-selective deposit feeding by the trace maker accounts for the redistribution of the silt- and clay-sized fraction (<40 µm in grain diameter) and relative enrichment of organic material (Figs. 2B and 2C). The average TOC values for the burrow core (1.8 wt%) were determined to be 1.0 wt% higher than for unbioturbated host sediment (0.7 wt%) and 1.1 wt% higher than for the burrow halo (0.6 wt%). Average $\delta^{13}C_{org}$ values were found to be –24.4‰, with systematic variations of organic carbon quality between halo (–23.8‰) and burrow core (–24.4‰; $\Delta^{13}C_{org}$ ~0.6‰). Combined SRS-XRF (Fig. 3) and ICP-MS analyses (Fig. 4) reveal that within the burrow halo, redox-sensitive trace elements (including Rb and Zr) are depleted by 10%–20%, whereas the same elements appear to be enriched by 40%–80% in the burrow core. Conversely, Sr and Ba are depleted in both the halo and burrow core (Fig. 4A).

Using FTIR spectroscopy the fecal core was determined to be enriched in illite and/or smectite relative to host sediment and burrow halo (Fig. 4B). The 3620 cm^{-1} absorption band represents the OH stretch for hydroxyl bonded to a double Al-Al (Besson and Drits, 1997). Within the fecal burrow core, the peak broadening and attenuated intensities of XRD peaks characteristic of feldspar (25.6° and 28.5° 2θ) indicate alteration of clay- to silt-sized Ca-rich feldspar (Fig. 4C). Despite the presence of significant amounts of organic matter (TOC ~1.8 wt%) within the burrow core, both XRD and FTIR spectroscopy demonstrate the absence of the early diagenetic reaction products of organic carbon remineralization (e.g., pyrite, mackinawite, and greigite) in both the burrow halo and fecal core (Figs. 4B and 4C).

DISCUSSION

Food web experiments demonstrate that the isotopic composition of residual organic matter deviates from values expected from kinetic isotope fractionation effects alone (Landrum and Montoya, 2009; *contra* Hayes, 1993), yielding compounds with $\delta^{13}C_{org}$ values that are persistently lighter by -0.5‰ to -2‰ compared to the original ingested food. Future research will demonstrate whether isotopic fractionation is amplified or reduced in beds exhibiting a higher bioturbation intensity (cf. Harazim and McIlroy, 2015).

The rare pyrite in the burrow core is directly correlated with localized enrichment of Co, Ni, Cu, and Zn. These elements are preferentially incorporated into the pyrite lattice via trace metal pyritization (Huerta-Diaz and Morse, 1992).

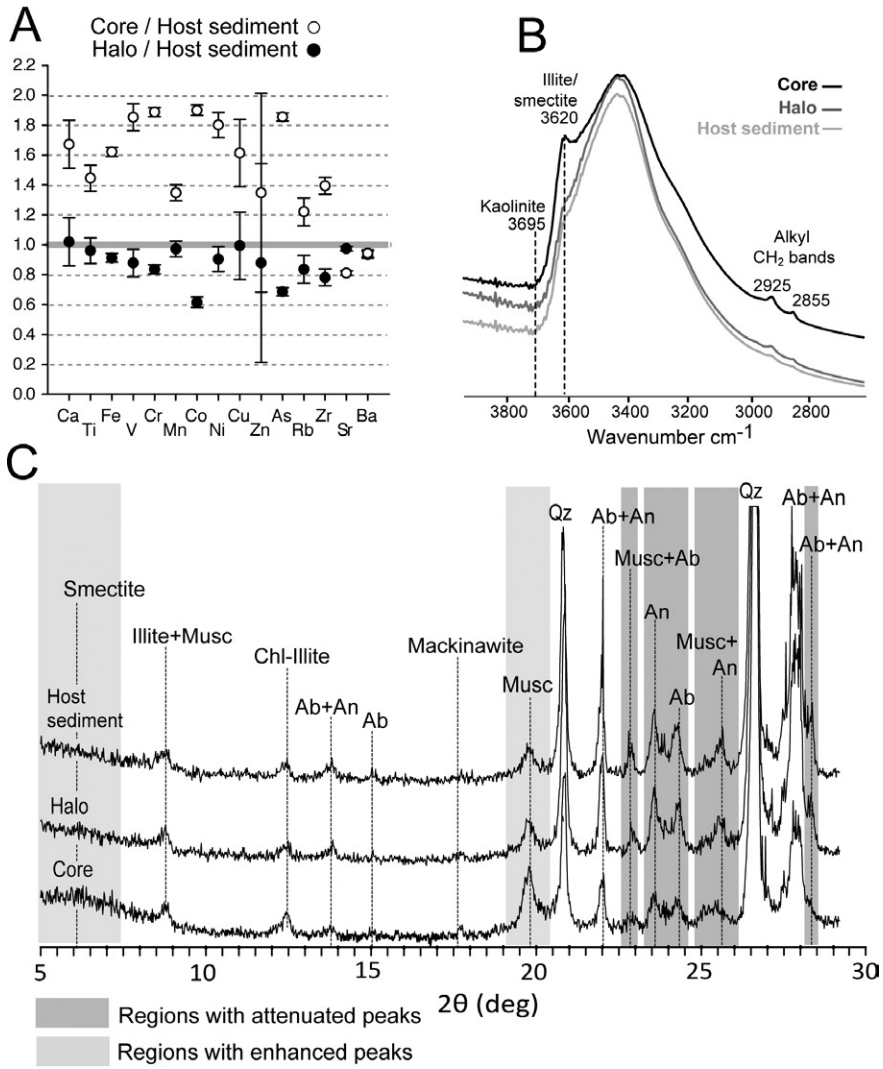

Figure 4. Inductively coupled plasma–mass spectrometry (ICP-MS), Fourier transform infrared analysis (FTIR), and X-ray diffraction (XRD) measurements for host sediment, burrow halo, and core, analyzed within this study (see the GSA Data Repository[1]). Samples were obtained from an entire hand sample. Aliquot comprised ~20 burrows. A: Relative enrichment/depletion of certain trace elements normalized to host sediment. Error bars report analytical precision. B: FTIR measurements. C: X-ray diffractograms (see text for discussion). Musc—muscovite; Chl—chlorite; Ab—albite; An—anorthite; Qz—quartz.

Some pyrite grains could have been ingested from the host sediment (see Izumi, 2014), though we consider the likelihood of such grains surviving the acidic portions of the gut unlikely. The abundant iron in the burrow cores (Fig. 3B) is mainly associated with smectite (Fig. 4B) or, potentially, with some lesser iron-rich dioctahedral mica. Because these ferrous iron–bearing silicate minerals are known to have low reactivity with H_2S (e.g., Canfield et al., 1992), they are unlikely to be an important source of iron for pyrite precipitation in the burrow core. The rarity of pyrite, together with the persistence of organic carbon in the fecal core, suggests that the carbon was most likely too refractory to fuel the formation of pyrite by bacterial sulfate reduction during early diagenesis (cf. Widerlund and Davison, 2007).

The near absence of pyrite in the burrow core suggests that the observed enrichment of transition metals within the fine-grained fecal burrow core is a result of an animal-sediment interaction. The partitioning of some elements in the phycosiphoniform burrows occurs without any bulk enrichment relative to the host sediment, inferring simple mechanical redistribution by the trace maker. Zirconium and Rb are significantly enriched in the fecal burrow core relative to the halo (by ~30%; Fig. 4A). Zirconium is concentrated in the heavy accessory mineral zircon, and Rb is most likely present as a trace element substituting for K within micas and feldspars. Neither element has any known biological importance, and as such, the relationship is likely to be simply due to grain-selective deposit feeding. Likewise, V and Cr are also most likely to be associated with phyllosilicates (Brigatti et al., 2003), consistent with the observed relative enrichment of dioctahedral mica in the burrow core relative to the burrow halo (Fig. 4C). In comparison, phosphorous is the only imaged element that does not co-vary with the spatial distribution of organic carbon (Fig. 3C). Phosphates and nitrates are important microbial nutrients, controlling microbial productivity in sediments (e.g., del Giorgio and Cole, 1998). Zones enriched in phosphorus surrounding *Planolites* isp. burrows (Fig. 3C) may reflect enhanced microbial productivity in the near-burrow environment caused by bioirrigation (cf. Herringshaw and McIlroy, 2013). In contrast, there is no enrichment in phosphorous associated with phycosiphoniform burrows (Fig. 3C), probably due to the deposit-feeding activity of the trace-making organism and absence of bioirrigation in its near-burrow environment.

While absolute element concentrations are controlled by the initial starting composition of the host sediment, they can also vary as a function of post-compaction mobility of certain elements during burial diagenesis. The measured concentrations of Sr and Ba indicate a significant depletion from both the burrow halo and fecal core. This trend cannot be explained by spatial mechanical redistribution of existing mineral phases (Fig. 2C). Because Ba and Sr are common components of biominerals such as teeth and shells, their depletion in the burrow relative to the host sediment might be explained by biomineralization (e.g., Lowenstam, 1981). Alternatively, feeding activity of macroorganisms is capable of degrading unstable minerals (e.g., biotite and chlorite) and feldspars (McIlroy et al., 2003).

A combination of techniques (XRD, FTIR, SEM) demonstrates that there is some preferential weathering of grains in the fecal core of the burrows (Figs. 2 and 4), and authigenic clay minerals absent in the host sediment are found there (Fig. 2D). The fecal core of the burrow also contains altered silt-sized lithic fragments and feldspars. Peak broadening in the XRD traces of plagioclase and albite (Fig. 4C) indicates weathering and may explain the mass balance deficit of Sr and Ba within the burrow fecal core. When weathered, feldspars and other detrital minerals rich in Sr and Ba release high-ionic-radius elements from their crystal lattices as they alter to illite and/or smectite (Drake and

[1]GSA Data Repository item 2015338, isotope ratios and elemental concentrations of total organic carbon, and trace element concentrations of host sediment, burrow halo, and core, is available online at www.geosociety.org/pubs/ft2015.htm, or on request from editing@geosociety.org or Documents Secretary, GSA, P.O. Box 9140, Boulder, CO 80301, USA.

Weill, 1975). Illite and smectite are both present in abundance in the fecal burrow core. The liberation of Sr and Ba is a result of their large atomic radii, too large to fit into the authigenic illites and smectites produced by biological weathering. This weathering is likely to have occurred partly in the gut of the trace maker (e.g., McIlroy et al., 2003), meaning that Sr and Ba are likely to have been released into the gut environment and, if not metabolized (or biomineralized), subsequently expelled into the pore waters of the host sediment. In contrast, elements with small ionic radii (i.e., Ca) are likely to be incorporated into authigenic minerals, and thus remain fixed in the fecal burrow core.

CONCLUSION

This study has demonstrated that grain-selective deposit-feeding organisms significantly affect the distribution and concentrations of elements in mudstones in a number of ways.

Deposit feeders affect the concentration of redox-sensitive elements in mudstones through grain-selective sorting of detrital crystalline and amorphous components. In the absence of biologically reactive organic matter, these elements are considered to be incorporated into silicates, rather than into pyrite and organic matter.

The trace elements Sr and Ba, released by biological weathering of feldspars and lithic clasts, can be either incorporated into the vagile endobenthic organism itself and incorporated into biominerals, or lost to adjacent pore waters during or shortly after egestion.

The relationship between bioturbation and elemental distributions in mudstones documented herein underlines that the practice of bulk-rock geochemical analysis must be complimented with the elemental imaging of mudstone fabrics in order to quantitatively assess the potential for biogenic heterogeneity and elemental partitioning.

ACKNOWLEDGMENTS

DH acknowledges additional support from the American Association of Petroleum Geologists, the International Association of Sedimentologists, the Society for Sedimentary Geology, and the Geological Society of America. This work was supported by a Natural Sciences and Engineering Research Council of Canada Discovery Grant and CRC to McIlroy and NERC support to Manning, Edwards, and Wogelius. We thank the scientists and support engineers for their help and advice with elemental mapping at Stanford Synchrotron Radiation Lightsource (beam lines 2-3 and 6-2). Manning thanks the Science and Technology Facilities Council for fellowship support. We thank two anonymous reviewers, Nicolas Tribovillard, and editor Ellen Thomas for constructive suggestions that improved the quality of this manuscript.

REFERENCES CITED

Aller, R.C., and Rude, P.D., 1988, Complete oxidation of solid phase sulfides by manganese and bacteria in anoxic sediments: Geochimica et Cosmochimica Acta, v. 52, p. 751–765, doi:10.1016/0016-7037(88)90335-3.

Bednarz, M., and McIlroy, D., 2009, Three-dimensional reconstruction of "phycosiphoniform" burrows: Implications for identification of trace fossils in core: Palaeontologia Electronica, v. 12, 12.3.13A.

Besson, G., and Drits, V.A., 1997, Refined relationships between chemical composition of dioctahedral fine-grained mica minerals and their infrared spectra within the OH stretching region. Part I: Identification of the OH stretching bands: Clays and Clay Minerals, v. 45, p. 158–169, doi:10.1346/CCMN.1997.0450204.

Brigatti, M.F., Caprilli, E., Marchesini, M., and Poppi, L., 2003, The crystal structure of roscoelite-1*M*: Clays and Clay Minerals, v. 51, p. 301–308, doi:10.1346/CCMN.2003.0510306.

Callow, R.H.T., McIlroy, D., Kneller, B., and Dykstra, M., 2013, Ichnology of Late Cretaceous turbidites from the Rosario Formation, Baja California, Mexico: Ichnos, v. 20, p. 1–14, doi:10.1080/10420940.2012.734763.

Canfield, D.E., Raiswell, R., and Bottrell, S., 1992, The reactivity of sedimentary iron minerals toward sulfide: American Journal of Science, v. 292, p. 659–683, doi:10.2475/ajs.292.9.659.

del Giorgio, P.A., and Cole, J.J., 1998, Bacterial growth efficiency in natural aquatic systems: Annual Review of Ecology and Systematics, v. 29, p. 503–541, doi:10.1146/annurev.ecolsys.29.1.503.

Drake, M.J., and Weill, D.F., 1975, Partition of Sr, Ba, Ca, Y, Eu^{2+}, Eu^{3+} and other REE between plagioclase feldspar and magmatic liquid: An experimental study: Geochimica et Cosmochimica Acta, v. 39, p. 689–712, doi:10.1016/0016-7037(75)90011-3.

Edwards, N.P., et al., 2014, Leaf metallome preserved over 50 million years: Metallomics, v. 6, p. 774–782, doi:10.1039/C3MT00242J.

Harazim, D., and McIlroy, D., 2015, Mud-rich density-driven flows along an Early Ordovician storm-dominated shoreline: Implications for shallow-marine facies models: Journal of Sedimentary Research, v. 85, p. 509–528, doi:10.2110/jsr.2015.38.

Hart, B.S., Macquaker, J.H., and Taylor, K.G., 2013, Mudstone ("shale") depositional and diagenetic processes: Implications for seismic analyses of source-rock reservoirs: Interpretation (Tulsa), v. 1, p. B7–B26, doi:10.1190/INT-2013-0003.1.

Hayes, J.M., 1993, Factors controlling ^{13}C contents of sedimentary organic compounds: Principles and evidence: Marine Geology, v. 113, p. 111–125, doi:10.1016/0025-3227(93)90153-M.

Herringshaw, L.G., and McIlroy, D., 2013, Bioinfiltration: Irrigation-driven transport of clay particles through bioturbated sediments: Journal of Sedimentary Research, v. 83, p. 443–450, doi:10.2110/jsr.2013.40.

Hesselbo, S.P., Jenkyns, H.C., Duarte, L.V., and Oliveira, L.C., 2007, Carbon-isotope record of the Early Jurassic (Toarcian) Oceanic Anoxic Event from fossil wood and marine carbonate (Lusitanian Basin, Portugal): Earth and Planetary Science Letters, v. 253, p. 455–470, doi:10.1016/j.epsl.2006.11.009.

Huerta-Diaz, M.A., and Morse, J.W., 1992, Pyritization of trace metals in anoxic marine sediments: Geochimica et Cosmochimica Acta, v. 56, p. 2681–2702, doi:10.1016/0016-7037(92)90353-K.

Izumi, K., 2014, Utility of geochemical analysis of trace fossils: Case studies using *Phycosiphon incertum* from the Lower Jurassic shallow-marine (Higashinagano Formation, southwest Japan) and Pliocene deep-marine deposits (Shiramazu Formation, central Japan): Ichnos, v. 21, p. 62–72, doi:10.1080/10420940.2013.877008.

Jenkyns, H.C., 2010, Geochemistry of oceanic anoxic events: Geochemistry Geophysics Geosystems, v. 11, Q03004, doi:10.1029/2009GC002788.

Jenner, G.A., Longerich, H.P., Jackson, S.E., and Fryer, B.J., 1990, ICP-MS—A powerful tool for high-precision trace-element analysis in Earth sciences: Evidence from analysis of selected U.S.G.S. reference samples: Chemical Geology, v. 83, p. 133–148, doi:10.1016/0009-2541(90)90145-W.

Landrum, J.P., and Montoya, J.P., 2009, Organic matter processing by the shrimp *Palaemonetes* sp.: Isotopic and elemental effects: Journal of Experimental Marine Biology and Ecology, v. 380, p. 20–24, doi:10.1016/j.jembe.2009.08.020.

Lowenstam, H.A., 1981, Minerals formed by organisms: Science, v. 211, p. 1126–1131, doi:10.1126/science.7008198.

McIlroy, D., Worden, R.H., and Needham, S.J., 2003, Faeces, clay minerals and reservoir potential: Journal of the Geological Society, v. 160, p. 489–493, doi:10.1144/0016-764902-141.

Poduska, K.M., Regev, L., Boaretto, E., Addadi, L., Weiner, S., Kronik, L., and Curtarolo, S., 2011, Decoupling local disorder and optical effects in infrared spectra: Differentiating between calcites with different origins: Advanced Materials, v. 23, p. 550–554, doi:10.1002/adma.201003890.

Ratcliffe, K.T., Wright, A.M., and Schmidt, K., 2012, Application of inorganic whole-rock geochemistry to shale resource plays: An example from the Eagle Ford Shale Formation, Texas: The Sedimentary Record, v. 10, p. 4–9, doi:10.2110/sedred.2012.2.4.

Widerlund, A., and Davison, W., 2007, Size and density distribution of sulfide-producing microniches in lake sediments: Environmental Science & Technology, v. 41, p. 8044–8049, doi:10.1021/es071510x.

Wogelius, R.A., et al., 2011, Trace metals as biomarkers for eumelanin pigment in the fossil record: Science, v. 333, p. 1622–1626, doi:10.1126/science.1205748.

Zhu, Q., Aller, R.C., and Fan, Y., 2006, Two-dimensional pH distributions and dynamics in bioturbated marine sediments: Geochimica et Cosmochimica Acta, v. 70, p. 4933–4949, doi:10.1016/j.gca.2006.07.033.

Manuscript received 31 May 2015
Revised manuscript received 6 September 2015
Manuscript accepted 13 September 2015

Printed in USA